# Polydopamine treatment of chitosan nanofibers for the conception of osteoinductive scaffolds for bone reconstruction

Syrine Dimassi, Nicolas Tabary, Feng Chai, Cedric Zobrist, Jean-Christophe Hornez, Frederic Cazaux, Nicolas Blanchemain, Bernard Martel

# Polydopamine treatment of chitosan nanofibers for the conception of osteoinductive scaffolds for bone reconstruction

Syrine Dimassi[a], Nicolas Tabary[a], Feng Chai[b], Cédric Zobrist[a], Jean-Christophe Hornez[c], Frédéric Cazaux[a], Nicolas Blanchemain[b] and Bernard Martel[a*]

[a] Univ. Lille, CNRS, INRA, ENSCL UMR8207, UMET – Unité Matériaux et Transformations, Lille, France
[b] Univ. Lille, INSERM, CHU Lille, U1008 – Controlled Drug Delivery Systems and Biomaterials, Lille, France
[c] Université Polytechnique Hauts de France, LMCPA, Maubeuge, France

*Corresponding authors:
Bernard Martel; E-mail address: bernard.martel@univ-lille.fr

## Abstract

We report the influence of treatment time of electrospun chitosan nanofibers (CHT NFs) in dopamine hydrochloride bath (2 mg. mL -1 in 10 mM Tris buffer, pH 8.5) on the extent of the polydopamine (pDA) coating on NFs surface. The reaction was characterized by FTIR and SEM analysis and the cytocompatibility of the scaffolds toward MT3C3-E1 cells was assessed. Biomimetic deposition of hydroxyapatite (HA) in 1.5xSBF batch was investigated by SEM-EDS and XRD. Samples treated in dopamine bath during 2 h promoted the structural stability of NFs in PBS, provided optimal cytocompatibility and induced the in vitro biomineralization from 6 days in 1.5xSBF. The XRD and SEM-EDS investigations confirmed formation of spherical-shaped particles composed of apatitic phase. Finally, this study shows that these NFs-pDA scaffolds prepared in the optimal experimental conditions defined here are promising candidates for application as osteoinductive scaffolds for bone regeneration applied to orthopaedic and dental applications

*Keywords: electrospinning; nanofibers; polydopamine; scaffolds; hydroxyapatite; bone tissue engineering*

## 1. Introduction

Bone tissue engineering (BTE) has been discovered in the 1990s and its interest has grown exponentially over the years. It holds a great promise for the treatment of bone diseases or defects (Ranganathan, Balagangadharan & Selvamurugan, 2019). One of the main components of BTE is the scaffold that should mimic the extracellular matrix (ECM) and provide a three-dimensional environment for cells and biological molecules to grow and regenerate tissue (Ehrbar, Lütolf, Rizzi, Hubbell & Weber, 2008). Thus, 3D-scaffold should have a highly porous structure with interconnected

pores and an extremely large specific surface area (Liu, Cui, Zhuang, Wei & Chen, 2014). Various methods for fabrication of porous scaffolds that mimics the natural ECM are developed, such as phase separation (Ciapetti et al., 2012; Salerno, Fernández-Gutiérrez, San Román del Barrio & Domingo, 2015), freeze-drying (Chong, Zarith & Sultana, 2015; Flores et al., 2016; Shahbazarab, Teimouri, Chermahini & Azadi, 2018) , auto-assembly (Nie, Li, Lu, Lei, Zhang & Wang, 2013; Pan, Chen, Metavarayuth, Su & Wang, 2018) and electrospinning (Chen et al., 2017; Jang, Castano & Kim, 2009; Liao, Murugan, Chan & Ramakrishna, 2008; Sharifi, Atyabi, Norouzian, Zandi, Irani & Bakhshi, 2018).

Electrospinning, a relatively simple and useful fabrication technique, is extensively used to manufacture nonwoven mats of fibers with diameters ranging from several microns down to less than 100 nm (Chen, Li, Li & Xie, 2018; Wen, Zong, Linhardt, Feng & Wu, 2017). The intrinsic properties of resulted scaffolds offer a familiar environment to cells promoting their adhesion and proliferation. Further, it is possible to modulate nanofibers morphology, as the size of fibers diameters and the pores, by optimizing solution, process and/ or environmental parameters, and properties of scaffolds depending on biomaterial choice (Gupta, Haider, Choi & Kang, 2014; Haider, Haider & Kang, 2018; Kwak, Haider, Gupta, Kim & Kang, 2016)

Chitosan (CHT), a linear polysaccharide naturally present in fungi or obtained from deacetylation of chitin and made up of D-glucosamine and N-acetyl-D-glucosamine repeating units linked through β (1,4)- linkages, has emerged as a promising candidate for bone tissue engineering. Indeed, CHT has a similar structure to that of bone extracellular glycosaminoglycan and thus presents various properties such as biocompatibility, non-toxicity, biodegradability, etc. (Balagangadharan, Dhivya & Selvamurugan, 2017; LogithKumar, KeshavNarayan, Dhivya, Chawla, Saravanan & Selvamurugan, 2016). Studies have reported that CHT plays an important role in the enhancement of cell adhesion and proliferation, osteoblast differentiation and mineralization (Balagangadharan, Dhivya & Selvamurugan, 2017; LogithKumar, KeshavNarayan, Dhivya, Chawla, Saravanan & Selvamurugan, 2016; Pattnaik, Nethala, Tripathi, Saravanan, Moorthi & Selvamurugan, 2011; Sainitya et al., 2015; Saravanan, Nethala, Pattnaik, Tripathi, Moorthi & Selvamurugan, 2011). Nevertheless, CHT needs to be associated with other polymers (natural or synthetic ones), metals and/or ceramics in order to promote its properties as mechanical strength and structural integrity for BTE applications. First of all, for processing CHT by electrospinning, it has to be mixed with a non-ionic polymer such as polyethyleneoxide (PEO) for promoting chains entanglements and thus facilitate electrospinning process (Frohbergh et al., 2012; Jiang, Deng, James, Nair & Laurencin, 2014; Khajavi, Abbasipour & Bahador, 2016; Levengood & Zhang, 2014; Norowski Jr et al., 2015; Shalumon, Sowmya, Sathish, Chennazhi, Nair & Jayakumar, 2013; Van Hong Thien, Hsiao, Ho, Li & Shih, 2013; Yang, Chen & Wang, 2009). In addition, if CHT nanofibers provide the structural properties for BTE applications, it

does not intrinsically present osteoinductive properties. Therefore, chitosan nanofibers are often chemically modified after their spinning, or used in combination with other materials that provide the biochemical cues for acceleration of bone regeneration. (Balagangadharan, Dhivya & Selvamurugan, 2017).

Globally, functionalization of biomaterials promoting the pre-osteoblast cells proliferation and mineralization process has been extensively studied in literature, (Bose, Robertson & Bandyopadhyay, 2018; Hu, Ashok, Nisbet & Gautam, 2019; Jiao & Cui, 2007). Biomineralization is a regulated process by which living organisms produce mineral phase composed of calcium phosphate, which is an essential requirement for the normal skeletal development of bone tissue. Therefore, studies have been conducted to promote the growth of apatitic phase (most commonly hydroxyapatite) at the surface and within the bone matrix. This would promote adhesion, proliferation and differentiation of bone cells, and thus stimulate bone formation and regeneration of natural bone tissue. Therefore, many investigations have reported the use of a simple, effective and bio-inspired strategy that consists of the functionalization of biomaterials with polydopamine (pDA), that has generated a great interest in several areas of nanomedicine, from biosensors to tissue engineering (Ho & Ding, 2014; Lee *et al.*, 2016; Lynge, van der Westen, Postma & Städler, 2011; Tsai, Chen, Chien, Kuo & Wang, 2013). Ko *et al.* studied the grafting of peptides derived from bone morphogenetic factor 2 (BMP-2) on PLGA films functionalized with pDA. They demonstrated the ability of these materials to regulate osteogenic differentiation and *in vitro* and *in vivo* mineralization of human adipose stem cells (hADSC) (Ko, Yang, Shin & Cho, 2013). Similarly, Cho et al. have described the immobilization of BMP-2 growth factors on the surface of PCL nanoparticles coated with pDA to improve bone regeneration *in vivo* (Cho et al., 2014). Kwon *et al.* treated polyetheretherketone (PEEK) surface with pDA for the covalent immobilization of collagen or insulin. They report that this treatment increased the bioactivity of the PEEK surface allowing for adhesion, proliferation and osteogenic differentiation of MC3T3-E1 cells which could enhance tissue integration of biomedical implants (Kwon, Kim, Gupta & Kang, 2018).

Ryu et al. have introduced a universal biomineralization pathway capable of forming hydroxyapatite crystals on the surface of various materials, including ceramics, noble metals, semiconductors and synthetic polymers. They showed that catecholamine groups present in pDA were responsible for the adhesion and nucleation of hydroxyapatite in the presence of $Ca^{2+}$ ions at the interface. After incubation for two weeks in a simulated body fluid (SBF), the functionalized titanium metal implant was completely and uniformly covered with calcium phosphate (CaP) minerals, unlike virgin biomaterial (Ryu, Ku, Lee & Park, 2010). Introduced for the first time by Kokubo *et al.* to evaluate the surface changes of bioactive bioceramics (Kokubo, 1991), it is widely used as an *in vitro* characterization method to study apatite layer formation on the surface of implants and thus predict their osteoinductive properties *in vivo* (Chen, Nouri, Li, Lin, Hodgson & Wen, 2008; Kokubo & Takadama, 2006).

In particular, very few papers report the pDA treatment of electrospun materials intended for biomedical applications. Very recently, Ma et al. (Ma et al., 2021) and Zia et al. (Zia, Tabassum, Meng, Xin, Gong & Li, 2021) reported the treatment of electrospun substrates with pDA for promoting the immobilization of chitosan on the NFs forming functional coatings providing anti bacterial activity and heavy metal ions sorption, respectively. Interestingly, Ziu *et al.* reported the elaboration of a composite PLLA-CHT interpenetrated fibrous network treated with pDA that displayed enhanced mechanical properties and osteogenic activity (Liu et al., 2017).

If the treatment of nanofibrous electrospun scaffolds by pDA for biomedical (and other) applications have been already reported in literature, the former studies do not discuss the influence of the parameters of the pDA treatment step on the subsequent steps for their functionalization neither on their intrinsic physicochemical nor biological properties. Therefore, in this paper we report in depth the influence of the time of treatment of CHT NFs in the dopamine solution on the chemical composition of the NFs, and we aimed to define the optimal compromise between the pDA treatment time and i) the stability of the NFs in aqueous medium, ii) the cytocompatibility toward pre-osteoblasts MC3T3-E1 and iii) the capacity to promote the nucleation of hydroxyapatite. The results obtained showed that the materials obtained in optimized experimental conditions of pDA treatment display promising properties for use in tissue engineering and especially as scaffolds for bone reconstruction.

## 2. Materials and methods

### 2.1. Materials

Chitosan (CHT), low molecular weight grade batch WA1603121, 98.26% degree of deacetylation, was supplied by WISapple with a molecular weight of 200 000 $g.mol^{-1}$ (supplier values). Polyethylene oxide (PEO, 900 000 $g.mol^{-1}$), glacial acetic acid, phosphate buffered saline (PBS), dopamine hydrochloride and Trizma® base (Tris) were purchased from Sigma Aldrich (Saint-Quentin Fallavier, France).

All reagents were used as received from the manufacturer without further purification. Ultrapure water was used for all experiments (Veolia water aquadem, Purelab flex, ELGA, 18.2 MΩ).

### 2.2. Electrospinning process

CHT/PEO blend solutions were prepared at 3.3 wt % concentration, with a ratio CHT: PEO of 9:1, in 90% (v/v) acetic acid solution. The solution mixing was performed at room temperature with mechanical stirring of 300 rpm for 12 h to ensure complete dissolution of the solutes to obtain homogeneous solutions. The spun solution was filled into a 5 mL plastic syringe connected to a 21gauge needle through a polyethylene catheter (inner diameter 1 mm, VYGON) and placed onto a

syringe pump (Fisher Scientific). The electrospinning process was carried out at a flow rate of 0.3 $mL.h^{-1}$, a voltage between 12 and 15 kV and a tip-to-collector distance of 20 cm. Relative humidity and temperature were fixed at 33 ± 2 % and 21 ± 2°C, respectively. Nanofiber mats were collected on a roll collector (diameter 90 mm, rotation speed 150 rpm) and then thermally post-treated at 140 °C for 4 h under vacuum in order to improve their stability in aqueous medium.

## 2.3. Preparation of NFs pDA

The protocol described by Messersmith *et al.* has been adapted for the treatment of CHT NFs (Lee, Dellatore, Miller & Messersmith, 2007). We also relied on the work of Ryu *et al.* (Ryu, Ku, Lee & Park, 2010).The CHT/ PEO blend nanofibrous scaffolds were first cut into square shaped samples (4 x 4 cm) and immersed into dopamine hydrochloride solution (2 mg. $mL^{-1}$ in 10 mM Tris buffer, pH 8.5) at room temperature, under mechanical stirring and at open air conditions to promote dopamine's oxidation and polymerization. Different times of immersion were studied, ranging from 2 hours up to 5 days and the dopamine solution was renewed every day. Then, polydopamine coated samples (NFs pDA) were thoroughly rinsed with ultrapure water followed by three washes in an ultrasound bath to remove the unreacted dopamine and were air-dried for 24 h.

## 2.4. Characterization of functionalized scaffolds

### 2.4.1. Scanning Electron Microscopy

The morphological architectures of diverse membranes and scaffolds were observed using scanning electron microscopy (SEM) (Hitachi S-4700 SEM field emission GU) with an accelerating voltage of 5 kV and an emission current of 10 µA. All specimens were sputtered with a thin layer of chrome before imaging. Fibres diameter distribution and standard deviation were determined by ImageJ. Software using SEM images.

### 2.4.2. FTIR spectroscopy

Scaffolds were investigated by Attenuated Total Reflectance-Fourier Transformed Infrared (ATR-FTIR) using a PERKINELMER spectrometer (SpectrumOne) equipped with Spectrum software. Spectra were recorded from 4000 to 650 $cm^{-1}$ (Scan number of 16) with a resolution of 4 $cm^{-1}$.

### 2.4.3. Colorimetric quantification of amino groups

Density of surface amino groups of samples was carried out by performing a colorimetric assay with the sodium salts of orange II (Orange acid II, AO II, MW 350.32 g.mol-1, ≥ 85%, Sigma Aldrich™). An aqueous solution of AO II at $2.5 \times 10^{-2}$ $mol.L^{-1}$ was prepared in ultrapure water at pH 3 (adjusted with 0.5 $mol.L^{-1}$ of HCl solution. Each sample (disk of 11 mm in diameter) was impregnated in 10 mL of this solution, under orbital shaking of 70 rpm, at room temperature and protected from light, at least for 12 h. Samples were then washed three times (5 minutes each) in 20

ml of ultrapure water which pH has been adjusted to 3 with a HCl solution at 0.5 mol.$L^{-1}$ to remove excess of AO II. In order to release the adsorbed AO II, they were immersed in 10 mL of ultrapure water at pH 12 (adjusted with 0.5 mol.$L^{-1}$ NaOH) for at least 12 h at room temperature and under orbital agitation of 70 rpm and away from light. Then, the AO II concentration of solutions was determined by spectrophotometric titration with an UV-visible spectrometer at 485 nm after adjusting the pH to 3 by adding 1 mL of 0.1 mol.$L^{-1}$ HCl solution in each sample. The amount of amino groups grafted on the surface was calculated from a calibration curve generated with AO II solutions of known concentrations according to the following formula:

$$-NH_2\ (\mu mol.cm^{-2}) = \frac{Absorbance\ .Volume\ (mL)}{Slope\ (mL.\mu mol^{-1})\ .Surface\ (cm^2)}$$

### 2.4.5. Colorimetric quantification of catecholamine groups

Evidence of a pDA coating on raw scaffolds was reliably achieved using a simple and reliable method that is micro-bicinchoninic acid (micro-BCA assay). Investigations evidenced the success of detecting thin layers of pDA on different surfaces using this simple colorimetric test (Cho et al., 2014; Lih, Choi, Ahn, Joung & Han, 2016). Indeed, it is expected that amino groups of pDA can readily react with a bicinchoninic acid (BCA) based protein assay reagent, as when pDA-coated materials are exposed to test reagent, an attractive violet colour, due to the reduction reaction of $Cu^{2+}$ ions to $Cu^{+}$, is generated. Control (unmodified) and functionalized nanofibers of 6 mm diameter were placed into a microplate well (96 wells microplate), treated with 150 µL of the freshly prepared microBCA working reagent (as instructured by the manufacturer) (Thermofisher Scientific, France) and incubated for 2 h at 37°C. Absorbance was measured at 562 nm using a multiwall plate reader (microplate fluorometer (TwinkleTMLB 970; Berthold Technologies GmbH & Co, Germany).

### 2.4.6. Vapour sorption isotherms

The water sorption-desorption isotherms of samples were measured with a thermogravimetric analyser (Q5000 SA, TA Instruments, Guyancourt, France), consisting of a microbalance in which the sample and reference pans were enclosed in a humidity and temperature-controlled chamber. The relative humidity (RH) was controlled by mixing appropriate proportions (regulated by mass-flow controllers) of dry (RH=0%) and water saturated (RH=100%) $N_2$ gas flows (global flow set to 200 mL.$min^{-1}$) in the chamber. The temperature was controlled by Peltier elements.

Basically, the sample was first placed into the chamber and dried to 0% RH and 60°C until its weight was stabilized to 0.01% for 180 min. The chamber temperature was then decreased to 37°C and the humidity was increased stepwise with RH plateaus of 5% until RH value reached 95%. For each RH

plateau, the sample's weight was stabilized to 0.01% for a time period of 180 min. the water desorption isotherm was then registered by decreasing RH down to 0% with 5% RH increments.

### 2.5. *In vitro* biomineralization of scaffolds

1.5 x concentrated Simulated Body Fluid (1.5xSBF) solution was prepared according to Kokubo et al. (Kokubo & Takadama, 2006). Briefly, NaCl (213 mM), $NaHCO_3$ (6.3 mM), KCl (7.5 mM), $K_2HPO_4.3H_2O$ (1.5 mM), $MgCl_2.6H_2O$ (2.3 mM), $CaCl_2$ (3.8 mM), $Na_2SO_4$ (0.8 mM) and tris buffer (40 mM) were dissolved and stirred in ultrapure water. HCl (1 M) was added to the solution until reaching a pH of 7.4. Untreated and polydopamine treated nanofibers were immersed in 50 mL 1.5xSBF in a flat flask at 37°C. The 1.5xSBF was refreshed every two days. After incubation for 7 days, the scaffolds were taken out and gently washed with ultrapure water and air dried. The formation of apatite coating on the surface of polydopamine functionalized disks was observed using SEM (Hitachi S-4700 SEM field emission GU) at 5kV. Thermogravimetric analysis (TGA) was performed to highlight the presence of mineral phase within biomineralized scaffolds. Specifically, samples were placed into platinum pans and put into a TGA Q50 (TA Instruments), then heated from 30°C up to 700°C at a heating rate of 10 °C per minute under nitrogen protection (90 $mL.min^{-1}$). The crystalline phase of calcium phosphate precipitates was investigated by X-ray diffraction (XRD). XRD was performed using a X'Pert Pro MRD®, PANalytical. The diffractograms were obtained in the range of 5 to 70° (steps of 0.02°, counting time 120 s), with a detector (X'Celelerator®, PNAalyti-cal) provided with an anti-divergence slot 0, 5° and 1° and a mask of 10 mm.

### 2.6. *Cells proliferation test*

The proliferation of pre-osteoblast cell (MC3T3-E1, ATCC® CRL-2594TM, USA) on the surface of CHT nanofiber membranes was assessed by direct-contact experimental set-up. The CHT membrane disks (diameter 11 mm) were placed at the well bottom of 48 well cell culture multiwall plate and stabilized by rubber ring (Viton® O-rings, diameter 11 mm), and the well without membrane disk as control. 450 µL complete cell culture medium (CCM), which containing α-MEM (Gibco, France) with 10% fetal bovine serum (Gibco, France) and 40 µg/mL gentamicin (Panpharma, France), was added to each well. Then a 50 µL drop cell suspension (at $1.6\times10^5$ cells/mL) of MC3T3-E1 cells were seeded in each well. The culture plate was incubated at 37°C, 5% $CO_2$ and 100% humidity for 3 days. The cellular viability was measured by the AlamarBlue® assay (ThermoFisher Scientific, France). Briefly, the CCM was removed from each well, and 500 µL of 10% AlamarBlue® in CCM was added, and incubated for 2 h avoiding the light. From each well, 150 µL AlamarBlue® solution was transferred into a 96-well plate (Fluoro–LumiNunc™, ThermoScientific, Illkirch-Graffenstaden, France). The intensity of fluorescence was determined using a Twinkle LB 970 Microplate Fluorometer (Berthold, Bad Wildbad, Germany) with an excitation wavelength of 530 nm and an emission wavelength of 590

nm. The cell survival rate was expressed by the percentage of cell viability with respect to the value of the control.

## 3. Results and discussion

### 3.1. Characterization of raw CHT nanofiber membranes

Electrospun CHT/ PEO nanofibrous scaffolds before and after crosslinking step by thermal treatment (140°C, 4h) are shown in Fig. 1.a. Bead-free nanofibers with average diameter of CHT/ PEO nanofibers present low polydispersity (247 ± 36 nm). However, as spun NFs in PBS solution (pH 7.4) swelled, merged and shrunk upon drying, leading to the decrease of the nanofiblous mats porosity (Fig. 1.a.c). On contrary, as displayed in Fig. 1.a.d, the nanofibrous structure of samples post-treated at 140 °C for 4 hours was not affected. In the present case, the enhanced stability of the NFs in water after thermal treatment suggests the physical self-crosslinking of CHT. It is supposed that thermal treatment induced the dehydration of CHT within the NFs, promoting interchain hydrogen bondings, enhancing thereby NFs stability in PBS medium.

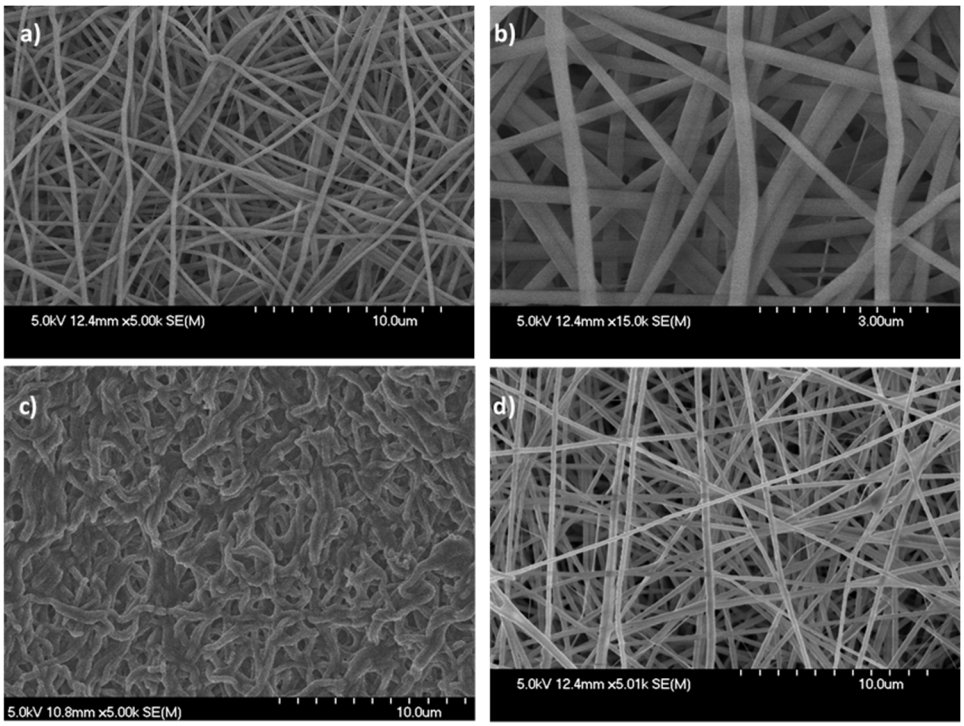


**Figure 1** SEM images of CHT/PEO based nanofibers with a mass ratio of 90/10, a) before × 5k; b) × 15k; c) after immersion in PBS solution at pH 7.4 for 24h (x5k) before (c) and after (d) thermal treatment (TT) at 140° C for 4h after immersion in PBS (x5k).

### 3.2. Modification of CHT nanofibers with polydopamine

The polydopamine (pDA) deposit was first highlighted by the colour change of membranes, as the non-functionalized membrane darkened with increase of the immersion time in dopamine solution (see supplementary data, Fig. S1).

### 3.2.1. SEM analysis

SEM images shown in Fig. 2 displayed the preservation of nanofibers morphology and the porosity of the nanofibrous membrane even after immersion in dopamine solution and the increase of fibres mean diameter with time of functionalization, from 222 ± 50 nm for raw NFs, up to 489 ± 76 nm after 120 hours of treatment. In addition, Fig. 2 also displays pDA particles appearing on samples treated with dopamine from reaction times superior to 48 hours (Fig. 2.f, g and h), forming well visible aggregates after 96 and 120 hours of functionalization (Fig. 2.h and i). These results are in agreement with those obtained by Shin *et al.* who studied the chemical modification of PCL nanofibers by PDA and evidenced that the surface morphology was dependent on the concentration of dopamine solution (Shin, Jun, Lim, Rhim & Shin, 2013). Indeed, these authors reported that scaffolds that have been immersed in a 2 mg. $mL^{-1}$ dopamine solution contained very few pDA particles while a concentration of 20 mg. $mL^{-1}$ provided nanofibers with higher quantity of pDA particles aggregates. We observed the same phenomenon in our case, as the SEM images in Fig. 2 display the appearance of pDA nanoparticles in the range of 100 nm from 2 hours of treatment (indicated by the arrows on the micrographs), and these nanoparticles formed aggregates well visible on samples treated during 96 and 120 hours. This behaviour could be explained by the fact that dopamine spontaneously polymerizes on the nanofibers' surface by forming a thin layer of pDA, and that extending the treatment timeleaded to homopolymerization of dopamine and precipitation of the insoluble pDA nanoparticles, firstly isolated on the scaffolds for treatment time up to 72 hours, and then forming aggregates. As a result, in order to limit the pores clogging of the scaffolds by pDA aggregates, an immersion time inferior or equal to 72 hours has been applied at this stage of the study.

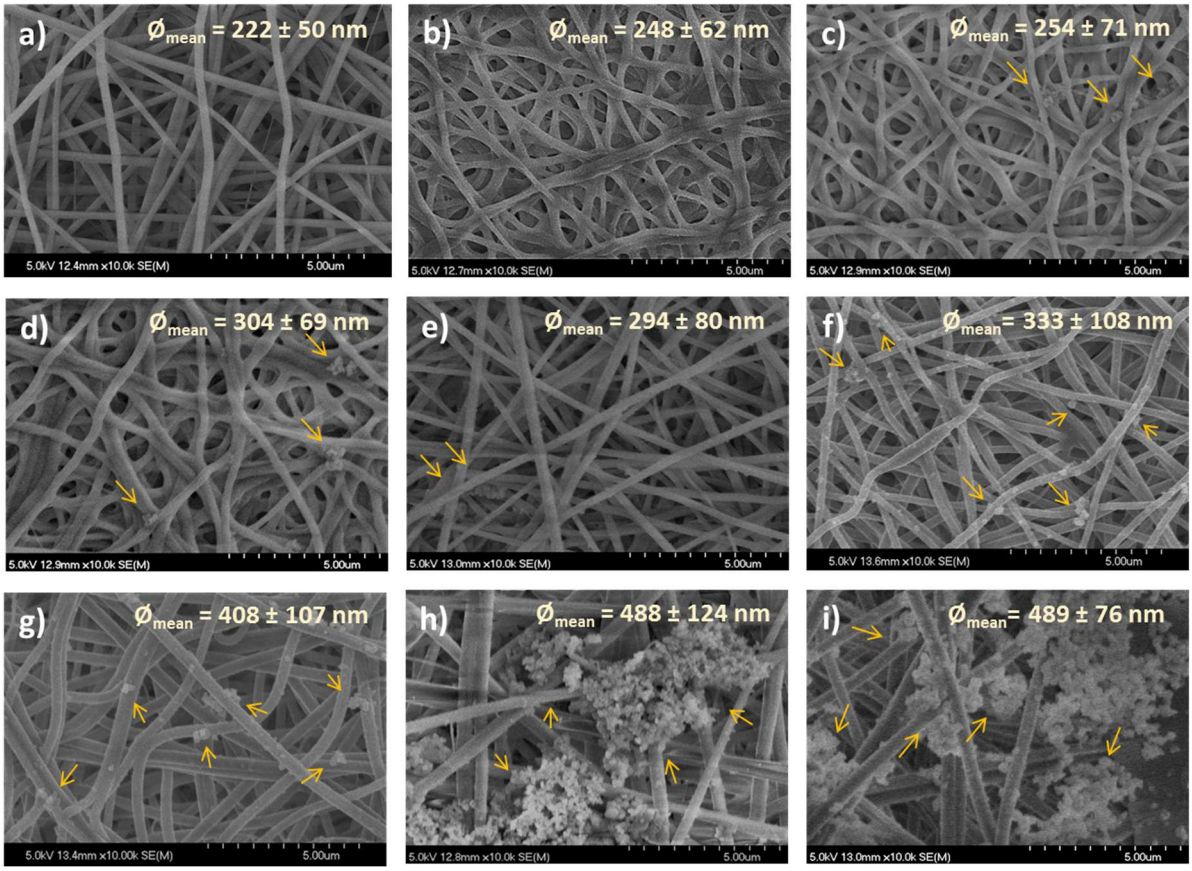


**Figure 2** SEM images (x10k) of CHT-based nanofibers a) non-functionalized and functionalized with polydopamine during b) 2h, c) 4h, d) 6h, e) 24h, f) 48h, g) 72h, h) 96h and i) 120h. The average diameters of NFs are indicated in the respective figures. Arrows indicate polydopamine particles on the surface of NFs

### 3.2.2. Characterization by FTIR

CHT-PEO (NFs CHT) and functionalized with pDA (NFs pDA) were characterized by attenuated total reflection mode (ATR) FTIR and spectra were compared with that of pDA powder synthesized in absence of NFs by self-polymerization of dopamine hydrochloride in pH 8.7 Tris buffer during 7 days. The black coloured precipitate in suspension was collected by filtration on 0.45µm membrane and analysed (Fig. 3). FTIR spectrum of CHT-based nanofibers displayed characteristic bands at 1653 $cm^{-1}$ and 1584 $cm^{-1}$ related to C=O elongation of amide groups (amide I band) and to N-H bending vibration of primary amines in the glucosamine repeat units of CHT, respectively. The N-H bending of amide groups (amide II band) appears at 1550 $cm^{-1}$, shouldering the band aforementioned. The band observed at 1370 $cm^{-1}$ corresponds to C-H symmetrical deformation of acetamide group, bands at 1062 and 1028 $cm^{-1}$ are related to the stretching of C-O and at 890 $cm^{-1}$ is related to the C-H bending out of the plane of the ring of monosaccharides (Dimzon & Knepper, 2015).

Compared to raw CHT nanofibers, pDA-functionalized scaffolds during 48 and 96 hours displayed increasing bands at 1598, 1428 and 1290 $cm^{-1}$ assigned to the overlap of C = C resonance vibrations

of aromatic cycles, and a peak at 1515 $cm^{-1}$ related to C - N vibrations confirming the presence of indole groups that are observed in the pDA nanoparticles' spectrum (Jiang, Zhu, Li, Xu & Zhu, 2010; Zangmeister, Morris & Tarlov, 2013). In addition, a decrease of the intensity of characteristic bands of CHT, in particular those at 1652 $cm^{-1}$ and at 1062 $cm^{-1}$, is observed. FTIR could not evidence the immobilization of pDA after 2 hours of treatment as spectra of raw and treated NFs were similar, however it confirmed the presence of pDA on the scaffolds at 48 hours.

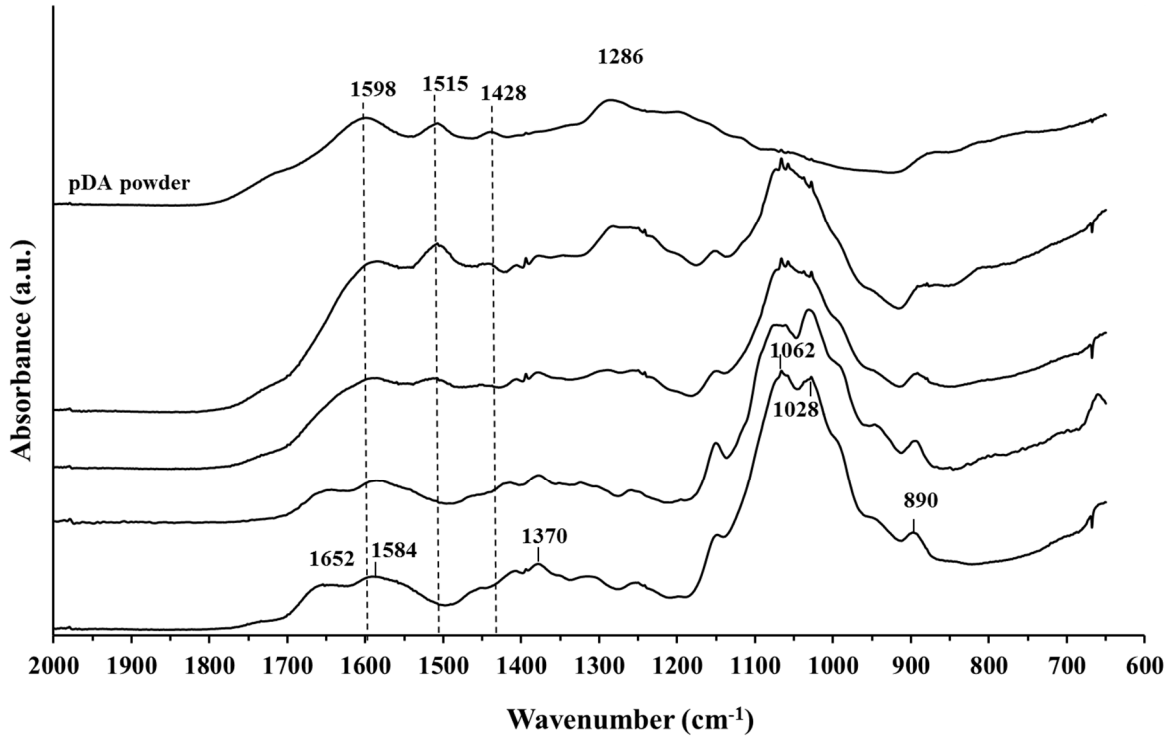


**Figure 3** IRTF-ATR spectra of raw chitosan-based nanofibers (NFs CHT), after functionalization with polydopamine (NFs pDA) during 2h, 48h and 96h and of polydopamine nanoparticles synthesized separately from NFs

### 3.2.3. Thermogravimetric analysis

Raw and functionalized membranes, as well as pDA powder were analysed by TGA **(see supplementary data, Fig. S2).** The thermogram of raw nanofibers showed a first mass loss between 25° C and 90° C related to the loss of water that has been absorbed by the scaffold. A second mass loss at 200 ° C corresponding to the degradation of both CHT and PEO can be observed, as well as a third mass loss at 320°C attributed to a coal residue degradation. The pDA powder exhibited a mass loss between 25°C and 80°C, due to dehydration, and a complete degradation in a single step ranging from 200°C up to 600°C. As a result, functionalized scaffolds displayed a first weight loss between 25 and 50°C attributed to water loss and a second one between 200°C and 500°C related to the degradation of

PEO, CHT and pDA. Compared to raw membranes, the functionalized ones showed a shift due to the decomposition of pDA that occurs at a higher temperature than that of CHT. It is worth to notice that the degradation of both samples was complete (no residue).

### 3.2.4. Titration of amino and catechol groups

As observed in Figs. 4.a and 4.b, a parallel evolution of amino groups and catechol groups occurred with reaction time. The amount of amino groups available on the surface of scaffolds was measured using the Orange II assay (Fig. 4.a). Unmodified nanofibers showed an amount of 2.0 $\mu mol.cm^{-2}$ of amino groups and this value increased up to 2.5 $\mu mol.cm^{-2}$ after 6h, 4.1 $\mu mol.cm^{-2}$ after 24h until reaching a maximum 4.6 $\mu mol.cm^{-2}$ at 72 h of scaffolds immersion in the dopamine solution. However, a surface modification higher than three days caused an insignificant decrease of the amount of free amino groups down to 4.2 $\mu mol.cm^{-2}$ after 120h. It is supposed that this phenomenon was due to the presence of polydopamine nanoparticles aggregates observed on SEM images in Fig. 2 that could reduce the availability toward Orange II of free amines present inside those aggregates.

Elsewhere, lower range of values of amino groups were measured by Kang *et al.* on bulk metal supports made of titanium and stainless steel (Kang et al., 2012). These authors reported presence of only 1.875 and 3.125 $nmol.cm^{-2}$ of amino groups respectively on smooth surfaces of titanium and stainless-steel treated by dopamine during 24h. Our group also reported similar results with the presence of 6.0 $nmol.cm^{-2}$ on vascular stents modified with pDA (Sobocinski et al., 2014). Such differences can be explained by the very higher specific surface of nanofibrous mats compared to that of smooth surfaces of bulk materials on the one hand, and also to the different surface reactivity of CHT toward dopamine, compared to metals.

The titration of catechol groups by the micro-BCA colorimetric test (Fig. 4.b) displays an increase from 0.048 to 0.131 $\mu mol.cm^{-2}$ for samples treated by dopamine during 2h and 72h respectively. Then, a slight decrease of catechol groups density for immersion times higher than 72h can be noticed, probably due to the presence of polydopamine aggregates formed in the nanofibrous network, as suggested above.

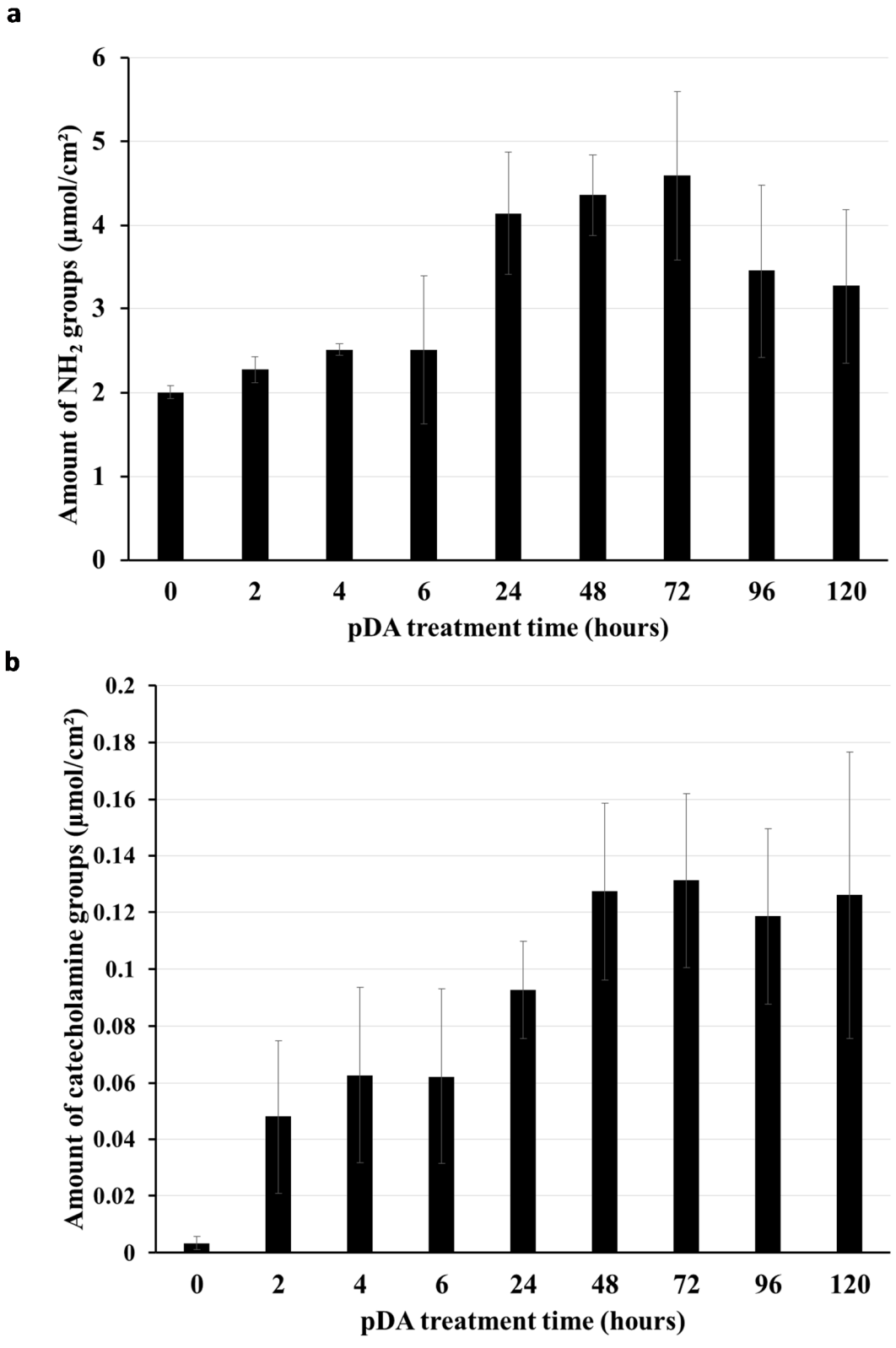


**Figure 4** Quantification expressed in µmol/cm² of amine groups (4.a) and catecholamine groups (4.b) on CHT NFs treated with different immersion times in polydopamine solutions ranging from 0h (control samples) up to 120h (n = 3).

### 3.2.5. Vapour sorption measurements

A water vapour sorption study was achieved on CHT/ PEO nanofibrous scaffolds before and after thermal post-treatment of NFs and after treatment with pDA (Fig. 5). Sorption and desorption curves displayed a similar behaviour with linear responses between 0% and 75% of relative humidity (RH), and exponential variation between 75% and 95% of humidity. A maximum of 435.6 mg and 459.8 mg of water uptake per gram of sample before and after thermal treatment, was respectively observed. Interestingly, water desorption cycle trace on untreated NFs was below that of adsorption while the opposite was observed on thermally treated NFs. This confirms that thermal treatment of NFs at 160°C induced a change of the physicochemical properties of NFs. Besides, the effect of polydopamine treatment on water vapour sorption of nanofibers was evidenced as observed in Fig. 1B. As a matter of fact, the water absorption and desorption measurements of unmodified and functionalized scaffolds by pDA are presented in Fig. 5. Water vapour uptake by membranes before and after pDA treatment decreased from 459.8 down to 322.3 mg of water / g of sample when HR was about 95%. For RHs between 0 and 80%, the two samples have similar water adsorption profiles, and above 80%, the moisture content of the CHT nanofibers has become greater than that of modified nanofibers. Consequently, this result shows that the functionalization step of CHT NFs by pDA has caused a decrease in NFs' swellability in water

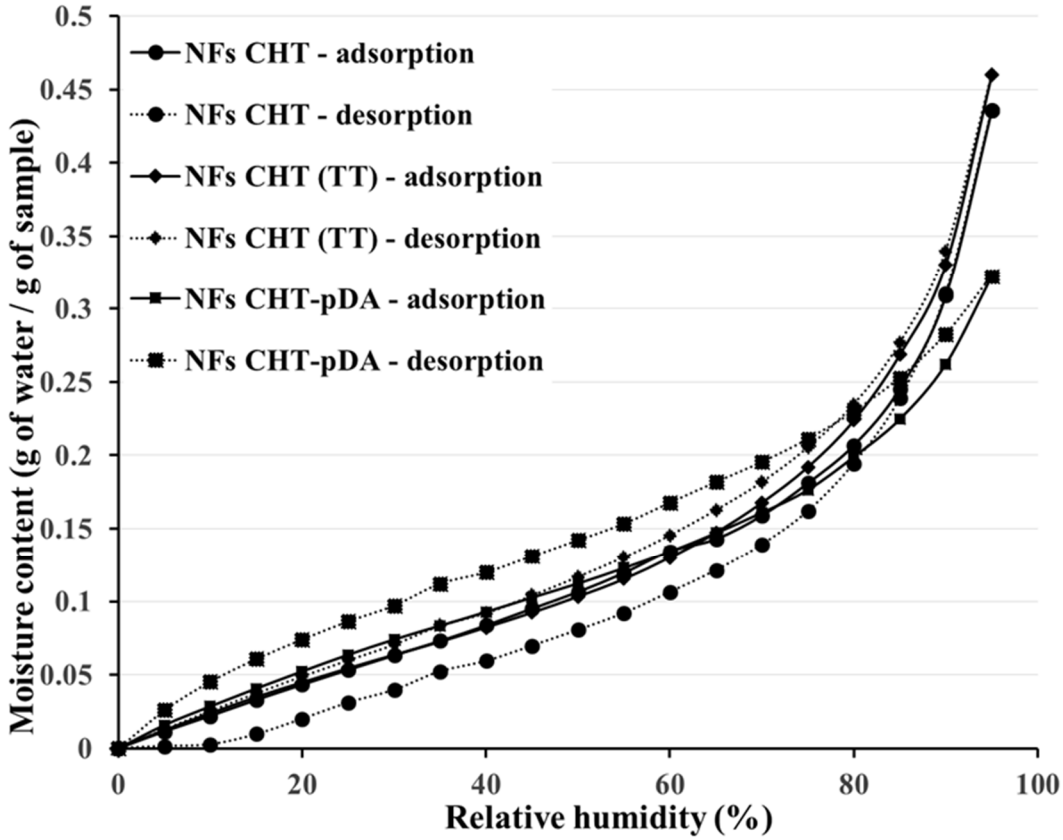


**Figure 5** Water vapor absorption isotherms of as spun CHT nanofibers before and after thermal treatment (TT) and after treatment with pDA

### 3.2.6. Degradation in PBS batch

Fig. 6.a shows the degradation profiles of the samples in PBS batch at 37°C. A first fast degradation phase, up to one day, and a second slower second phase can be observed of both profiles. In the first phase, a significant loss of mass of 8% and 2% for CHT NFs and CHT/ pDA NFs, respectively, was noticed. We previously reported that this weight loss could be assigned to the PEO dissolution in the PBS batch as CHT nanofibers were initially prepared from the electrospun solution containing 9:1 CHT-PEO weight ratio. This was evidenced by a proton NMR analysis of the freeze-dryed residue of the PBS degradation medium which displayed the NMR signal of PEO released from the CHT-PEO NFs (Ouerghemmi et al., 2016). Further, the kinetics of degradation process was slowed down after 10 days until reaching 10% and 6% of mass loss, respectively. Therefore, the polydopamine coating allowed to stabilize and delay degradation of nanofiber membranes. These results are confirmed by a SEM observation since swelling of CHT nanofibers could be observed at the beginning of the degradation (2 hours) (Fig. 6.b). While fibrous and porous morphology is retained for modified nanofibers that have lost their straightness.

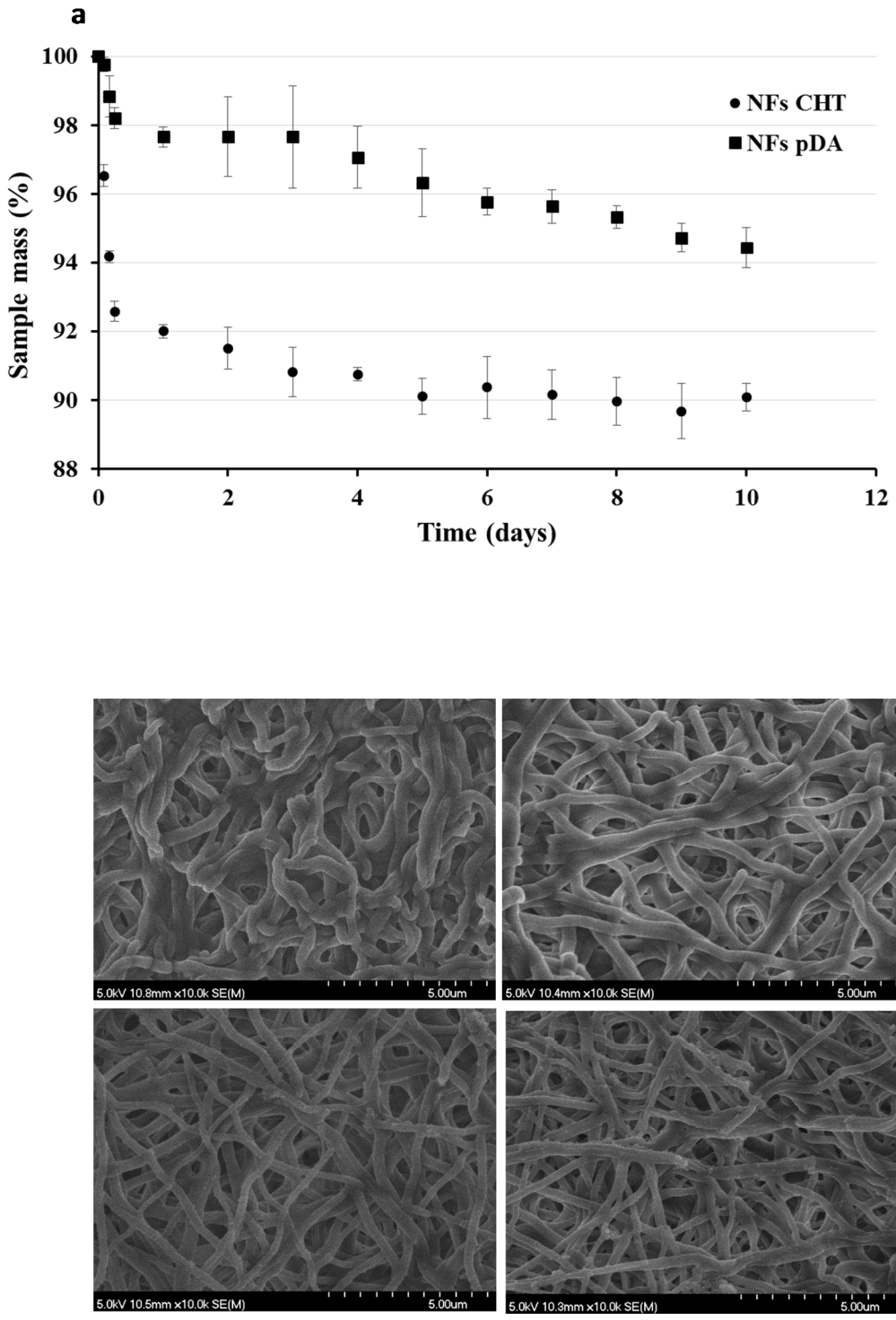


**Figure 6** Degradation of as spun and pDA functionalized nanofibers (n = 3) expressed by their weight percentage in function of time in PBS batch at 37°C (6.a), SEM images of samples after 2h and 5 days in PBS batch (x10k) (6.b).

### 3.2.7 Cytocompatibility study

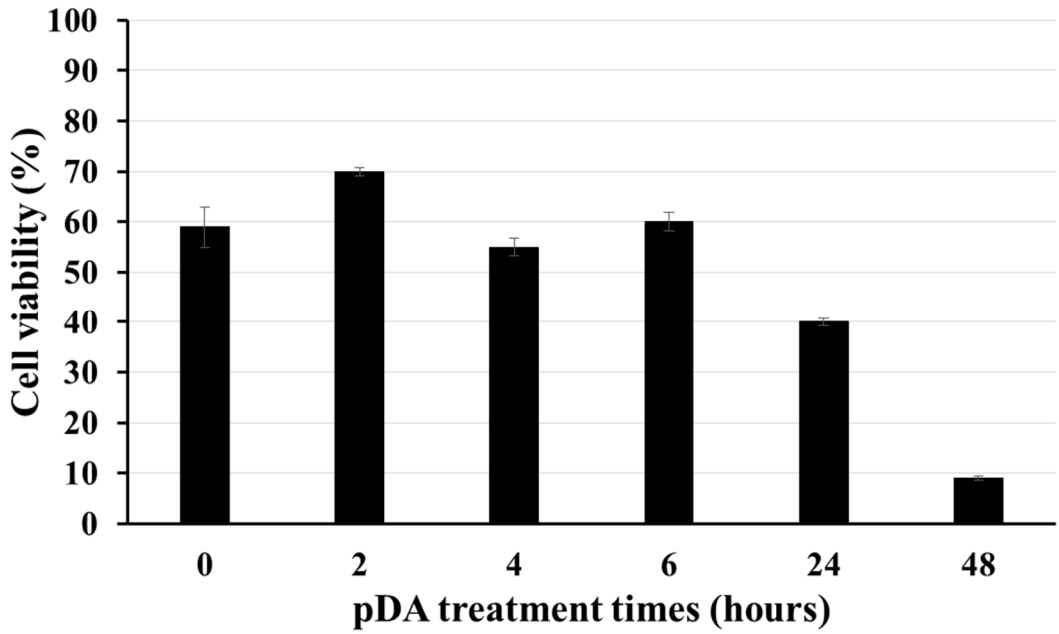


Figure 7 Viability of cells MC3T3-E1 in contact with NFs before (0h) and after pDA treatment during 2 to 48 hours by direct contact method (n=3) after 3 days of incubation. TCPS was used as control corresponding to a viability of 100%.

The cytocompatibility of samples treated with dopamine during times varying from 2 hours up to 48 hours was assessed in presence of MC3T3-E1 cells by the direct contact method. Figure 7 displays a cells viability of 70% for a treatment time of 2 hours, then viability decreased down to 60% after 6 hours, 40% after one day and levelled off at 8% after 2 days. It is known from literature that pDA especially in the shape of nanoparticles may provoke a cytotoxic effect. For example Nieto *et al*. studied in depth this phenomenon with tumor cells cultures (Nieto, Vega, Enrique, Marcelo & Martín Del Valle, 2019). As a matter of fact, the SEM study reported in an above section (Fig. 2) displayed the formation of pDA nanoparticles on NFs samples from reaction time of 4 hours in the dopamine batch. So this confirms that the decrease of the viability above 2 hours of treatment can be correlated with the formation of pDA nanoparticles. Finally, this experiment allowed us to fix the pDA treatment time to 2 hours for the preparation of scaffolds for their in vitro biomineralization described in the next section.

### 3.3. *In vitro* biomineralization of CHT-pDA scaffolds

The ability of the NFs to induce the formation of calcium phosphate (CaP) was evaluated *in vitro* by immersing the samples in a solution of 1.5×SBF for up to 7 days with renewing the solution every 48 h. Fig. 8.A displays that the surface of the nanofibrous scaffold previously functionalized with pDA for 2 h, is fully covered with spherical shaped CaP particles in contrast with the as spun CHT which does not display any particles formation (Fig. 8.A.a). As observed in Fig. 8.A.c), the spherical particles present a diameter in the range of 7 µm. Fig. 8B displays the evolution of NFs-pDA

scaffolds from the first to the seventh day in contact with SBF and evidences that biomineralization occurred from the 6th day.

After the complete pyrolysis of the organic part (CHT and pDA) observable up to 600°C, the TGA analysis of the biomineralized scaffolds displayed the presence of a mineral residue corresponding to 17% of the initial weight (See Fig. S3 in supplementary data).

Energy dispersive spectroscopy (EDS) microanalysis (Fig.8.C) displayed the presence of Ca and P elements on the biomineralized scaffolds. Calculated from their respective relative abundances the Ca/P ratio is 1.76. This value is close to that of hydroxyapatite whose Ca / P ratio is 1.67. Nevertheless, this study is semi-quantitative and does not allow us to affirm the presence of hydroxyapatite in its pure state.

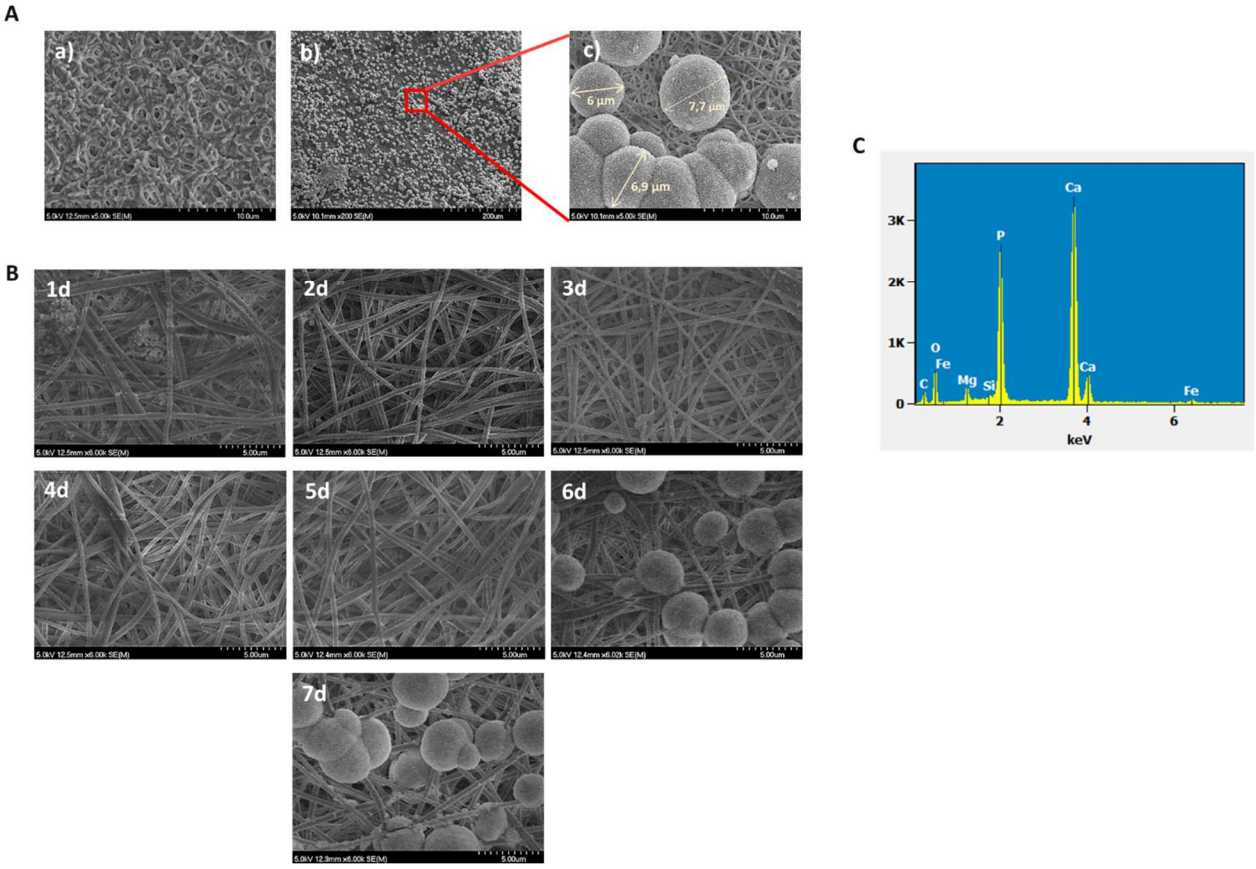


**Figure 8** SEM images of CHT nanofibers obtained after 7 days in SBF NFs as spun (without pDA coating) (magnification x5k) (8.A.a), NFs functionalized with pDA for 2h (magnification x200) (8.A.b), and (magnification x5k) (8.A.c) ; SEM images of nanofibers functionalized with pDA and then biomineralized for 1 up to 7 days (magnification x6k) (8.B); EDS spectrum of membranes after immersion in 1.5×SBF solution (8.C)

436 The biomineralized NFs surface was analysed by FTIR in total reflection mode (Fig. 9.a). The
437 spectrum of HA powder is also displayed in order to highlight its characteristic peaks.

438

439 Spectrum of NFs-pDA supporting CaP crystals displays a strong double band in the region 2920 -
440 2880 $cm^{-1}$ which can be attributed to $CH_2$ asymmetric and symmetric stretching, typical of
441 polysaccharides. However, in the lower region of the spectrum, the signal of the calcium phosphate
442 covering the scaffold overlaps the vibration bands relative to non-biomineralized NFs-pDA sample
443 (detailed in section 3.2.2 and Fig. 3). The vibrations bands of $\nu_3$ $PO_4^{3-}$ group (asymmetric elongation
444 of P-O) appears clearly at 1000-1100 $cm^{-1}$ (large band) and shouldering symmetric $\nu_1 PO_4^{3-}$ at 960 $cm^{-1}$
445 $^{1}$. The peak observed at 880 $cm^{-1}$ and the wide band at 1420-1470 $cm^{-1}$ reflect the presence of traces of
446 carbonate ions. The weak band at 1630 $cm^{-1}$ corresponds to free water (Kokubo & Takadama, 2006).

447 These results have been supplemented with a X-ray diffractometry (XRD) analysis in order to define
448 more finely the nature of the calcium phosphate nodules formed upon the biomineralization step. Fig.
449 9.b shows the different diffractograms of NFs after both pDA and biomineralization steps of the
450 process (green and blue plots respectively). A peak at $2\Theta = 20°$ corresponding to CHT (020 diffraction
451 plane), the main constituent of nanofiber scaffolds, was noticed and the shoulder observed at $2\Theta = 28°$
452 was attributed to PEO present in the precursor electrospun CHT solution (Ouerghemmi et al., 2016)

453

454 In addition, the spectrum of the mineral residue of biomineralized sample during 7days before (blue
455 plot) and after calcination (red plot) is displayed.

456 In addition, the diffractograms of biomineralized nanofibers before calcination (curve in blue) showed
457 a slight shoulder at $2\Theta=32°$ revealing the presence of an apatitic phase. The XRD spectrum of the
458 solid residue resulting from calcination of a biomineralized membrane (during 7d in 1.5xSBF) days
459 displayed well defined narrow peaks revealing the presence of a crystalline phase. As a matter of fact,
460 the spectrum of the calcined residue corresponds to a superposition of the spectrum of pure
461 hydroxyapatite (majority) as well as spectra of other calcium phosphates such as whitlockite and
462 magnesium and calcium phosphate (minor) (see supplementary data, Fig. S4 and Fig. S5). So, due to
463 the low percentage of crystallinity of the bio-mineralized phase it is not possible to correctly determine
464 the main angles and diffraction planes of this phase (blue plot), only the presence of chitosan seems
465 visible by XRD. However, after calcination at 1000 °C of biomineralized nanofibers (red plot) we
466 clearly see the peaks of calcium phosphate with the peak 100% of hydroxyapatite (plane 211, $2\Theta$ =
467 31.773 °) and the peak 100% of whitlockite (plane 0210, $2\Theta = 31.026$ °).

468
469

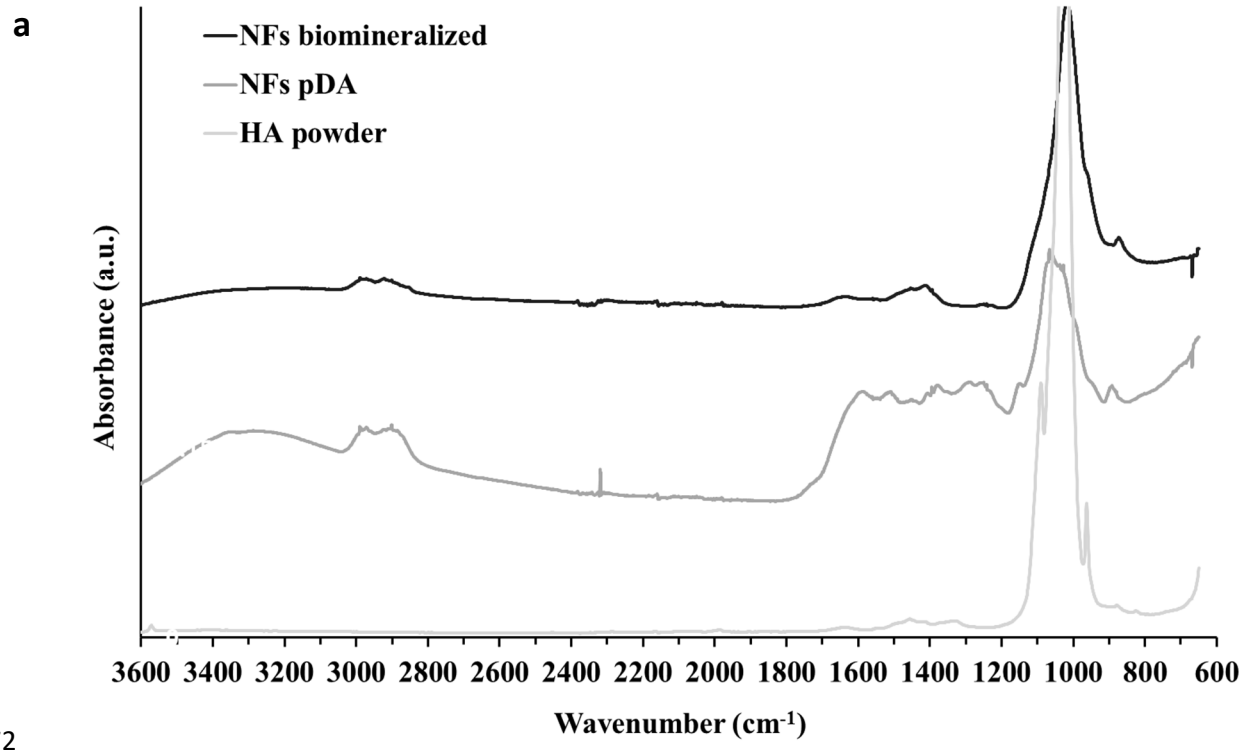


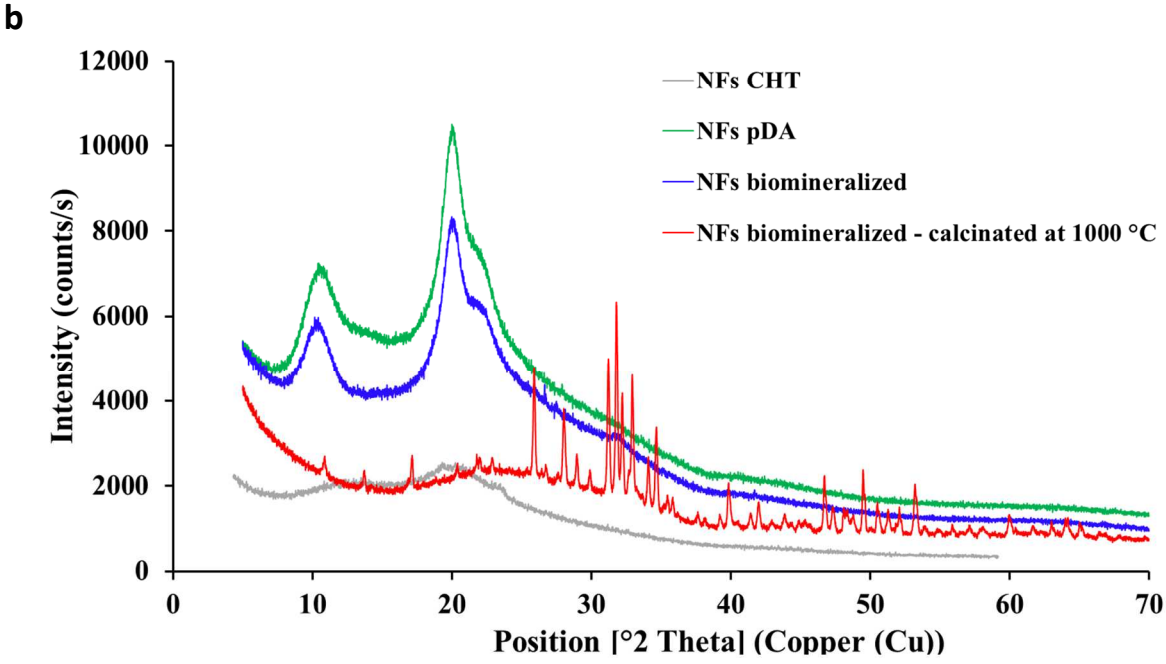


**Figure 9** IRTF-ATR spectra of pure powder of hydroxyapatite and nanofibers modified with pDA for 2h and after biomineralization during 7 days (9.a), Diffractograms of raw membranes (grey), functionalized nanofibers with pDA before (green) and after (blue) biomineralization process for 7d, calcination residue of biomineralized membrane after 7 d (red) (9.b).

## 4. Conclusion

This work firstly described the treatment of chitosan nanofibrous scaffolds by polydopamine (NFs-pDA) by applying increasing reaction times. FTIR and titration analyses displayed the increase of pDA layer on the CHT NFs up to 48 h. The SEM study revealed the presence of large pDA nanoparticles aggregates for treatment times more than 72 h. We observed that pDA treatment time of 2 h was the best compromise between i) the stabilization effect of NFs in PBS pH 7.4 medium, ii) the cytocompatibility in presence of MC3T3-E1 pre-osteoblast cells and iii) the ability of the scaffolds to biomineralize in 1.5xSBF medium.

As a matter of fact, after 6-day immersion in the 1.5xSBF solution, the formation of a mineralized layer composed of sphere-shaped nodules was observable by SEM. SEM-EDX and XPS analyses displayed this mineral phase was mainly composed of hydroxyapatite. The next steps of this study will be to study *in vitro* the proliferation, activity of alkaline phosphatase, osteogenesis-related proteins secretion of stem cells on the NFs-pDA scaffolds, and demonstrate thereby that this simple, bio-inspired surface modification of the NFs scaffold by pDA is a very encouraging tool for regulating cell behaviour, and may serve as an effective cell carrier for bone tissue engineering in the field of orthopaedic and dental applications. In particular, it will be interesting to investigate *in vivo* the process of bone reconstruction accomplished by the mineralisation process in concert with the biological action of bone-forming cells colonizing the scaffolds and the parallel progressive replacement of the bioresorbable NFs by new-formed bone.

## Acknowledgments

European Metropolis of Lille (MEL), Faculty of Sciences and Technologies of University of Lille, Region Hauts-de-France and Chevreul Institute (FR 2638) are acknowledged for supporting and funding this work.

## References

Balagangadharan, K., Dhivya, S., & Selvamurugan, N. (2017). Chitosan based nanofibers in bone tissue engineering. *International Journal of Biological Macromolecules, 104*, 1372-1382.

Bose, S., Robertson, S. F., & Bandyopadhyay, A. (2018). Surface modification of biomaterials and biomedical devices using additive manufacturing. *Acta Biomaterialia, 66*, 6-22.

Chen, S., Li, R., Li, X., & Xie, J. (2018). Electrospinning: An enabling nanotechnology platform for drug delivery and regenerative medicine. *Advanced Drug Delivery Reviews, 132*, 188-213.

Chen, X., Nouri, A., Li, Y., Lin, J., Hodgson, P. D., & Wen, C. e. (2008). Effect of surface roughness of Ti, Zr, and TiZr on apatite precipitation from simulated body fluid. *Biotechnology and Bioengineering, 101*(2), 378-387.

514 Chen, Z., Song, Y., Zhang, J., Liu, W., Cui, J., Li, H., & Chen, F. (2017). Laminated electrospun nHA/PHB-
515 composite scaffolds mimicking bone extracellular matrix for bone tissue engineering. *Materials*
516 *Science and Engineering: C, 72*, 341-351.
517 Cho, H.-j., Madhurakkat Perikamana, S. K., Lee, J.-h., Lee, J., Lee, K.-M., Shin, C. S., & Shin, H. (2014).
518 Effective Immobilization of BMP-2 Mediated by Polydopamine Coating on Biodegradable
519 Nanofibers for Enhanced in Vivo Bone Formation. *ACS Applied Materials & Interfaces, 6*(14),
520 11225-11235.
521 Chong, L. H., Zarith, N. Z., & Sultana, N. (2015). Poly(Caprolactone)/chitosan-based scaffold using
522 freeze drying technique for bone tissue engineering application. *2015 10th Asian Control*
523 *Conference (ASCC)* (pp. 1-4).
524 Ciapetti, G., Granchi, D., Devescovi, V., Baglio, S. R., Leonardi, E., Martini, D., Jurado, M. J., Olalde, B.,
525 Armentano, I., Kenny, J. M., Walboomers, F. X., Alava, J. I., & Baldini, N. (2012). Enhancing
526 Osteoconduction of PLLA-Based Nanocomposite Scaffolds for Bone Regeneration Using Different
527 Biomimetic Signals to MSCs. *International Journal of Molecular Sciences, 13*(2).
528 Dimzon, I. K. D., & Knepper, T. P. (2015). Degree of deacetylation of chitosan by infrared
529 spectroscopy and partial least squares. *International Journal of Biological Macromolecules, 72*,
530 939-945.
531 Ehrbar, M., Lütolf, M. P., Rizzi, S. C., Hubbell, J. A., & Weber, F. E. (2008). Artificial extracellular
532 matrices for bone tissue engineering. *Bone, 42*, S72.
533 Flores, C., Degoutin, S., Chai, F., Raoul, G., Hornez, J.-C., Martel, B., Siepmann, J., Ferri, J., &
534 Blanchemain, N. (2016). Gentamicin-loaded poly(lactic-co-glycolic acid) microparticles for the
535 prevention of maxillofacial and orthopedic implant infections. *Materials Science and*
536 *Engineering: C, 64*, 108-116.
537 Frohbergh, M. E., Katsman, A., Botta, G. P., Lazarovici, P., Schauer, C. L., Wegst, U. G. K., & Lelkes, P. I.
538 (2012). Electrospun hydroxyapatite-containing chitosan nanofibers crosslinked with genipin for
539 bone tissue engineering. *Biomaterials, 33*(36), 9167-9178.
540 Gupta, K. C., Haider, A., Choi, Y.-r., & Kang, I.-k. (2014). Nanofibrous scaffolds in biomedical
541 applications. *Biomaterials Research, 18*(1), 5.
542 Haider, A., Haider, S., & Kang, I.-K. (2018). A comprehensive review summarizing the effect of
543 electrospinning parameters and potential applications of nanofibers in biomedical and
544 biotechnology. *Arabian Journal of Chemistry, 11*(8), 1165-1188.
545 Ho, C.-C., & Ding, S.-J. (2014). Structure, Properties and Applications of Mussel-Inspired
546 Polydopamine. *Journal of Biomedical Nanotechnology, 10*(10), 3063-3084.
547 Hu, C., Ashok, D., Nisbet, D. R., & Gautam, V. (2019). Bioinspired surface modification of orthopedic
548 implants for bone tissue engineering. *Biomaterials, 219*, 119366.
549 Jang, J.-H., Castano, O., & Kim, H.-W. (2009). Electrospun materials as potential platforms for bone
550 tissue engineering. *Advanced Drug Delivery Reviews, 61*(12), 1065-1083.
551 Jiang, J.-H., Zhu, L.-P., Li, X.-L., Xu, Y.-Y., & Zhu, B.-K. (2010). Surface modification of PE porous
552 membranes based on the strong adhesion of polydopamine and covalent immobilization of
553 heparin. *Journal of Membrane Science, 364*(1), 194-202.
554 Jiang, T., Deng, M., James, R., Nair, L. S., & Laurencin, C. T. (2014). Micro- and nanofabrication of
555 chitosan structures for regenerative engineering. *Acta Biomaterialia, 10*(4), 1632-1645.
556 Jiao, Y.-P., & Cui, F.-Z. (2007). Surface modification of polyester biomaterials for tissue engineering.
557 *Biomedical Materials, 2*(4), R24-R37.
558 Kang, J., Sakuragi, M., Shibata, A., Abe, H., Kitajima, T., Tada, S., Mizutani, M., Ohmori, H., Ayame, H.,
559 Son, T. I., Aigaki, T., & Ito, Y. (2012). Immobilization of epidermal growth factor on titanium and
560 stainless steel surfaces via dopamine treatment. *Materials Science and Engineering: C, 32*(8),
561 2552-2561.
562 Khajavi, R., Abbasipour, M., & Bahador, A. (2016). Electrospun biodegradable nanofibers scaffolds for
563 bone tissue engineering. *Journal of Applied Polymer Science, 133*(3).

564 Ko, E., Yang, K., Shin, J., & Cho, S.-W. (2013). Polydopamine-Assisted Osteoinductive Peptide
565 Immobilization of Polymer Scaffolds for Enhanced Bone Regeneration by Human Adipose-
566 Derived Stem Cells. *Biomacromolecules, 14*(9), 3202-3213.
567 Kokubo, T. (1991). Bioactive glass ceramics: properties and applications. *Biomaterials, 12*(2), 155-163.
568 Kokubo, T., & Takadama, H. (2006). How useful is SBF in predicting in vivo bone bioactivity?
569 *Biomaterials, 27*(15), 2907-2915.
570 Kwak, S., Haider, A., Gupta, K. C., Kim, S., & Kang, I.-K. (2016). Micro/Nano Multilayered Scaffolds of
571 PLGA and Collagen by Alternately Electrospinning for Bone Tissue Engineering. *Nanoscale*
572 *Research Letters, 11*(1), 323.
573 Kwon, G., Kim, H., Gupta, K. C., & Kang, I.-K. (2018). Enhanced Tissue Compatibility of
574 Polyetheretherketone Disks by Dopamine-Mediated Protein Immobilization. *Macromolecular*
575 *Research, 26*(2), 128-138.
576 Lee, H., Dellatore, S. M., Miller, W. M., & Messersmith, P. B. (2007). Mussel-Inspired Surface
577 Chemistry for Multifunctional Coatings. *Science (New York, N.Y.), 318*(5849), 426-430.
578 Lee, S. J., Lee, D., Yoon, T. R., Kim, H. K., Jo, H. H., Park, J. S., Lee, J. H., Kim, W. D., Kwon, I. K., & Park,
579 S. A. (2016). Surface modification of 3D-printed porous scaffolds via mussel-inspired
580 polydopamine and effective immobilization of rhBMP-2 to promote osteogenic differentiation
581 for bone tissue engineering. *Acta Biomaterialia, 40*, 182-191.
582 Levengood, S. K. L., & Zhang, M. (2014). Chitosan-based scaffolds for bone tissue engineering. *Journal*
583 *of Materials Chemistry B, 2*(21), 3161-3184.
584 Liao, S., Murugan, R., Chan, C. K., & Ramakrishna, S. (2008). Processing nanoengineered scaffolds
585 through electrospinning and mineralization suitable for biomimetic bone tissue engineering.
586 *Journal of the Mechanical Behavior of Biomedical Materials, 1*(3), 252-260.
587 Lih, E., Choi, S. G., Ahn, D. J., Joung, Y. K., & Han, D. K. (2016). Optimal conjugation of catechol group
588 onto hyaluronic acid in coronary stent substrate coating for the prevention of restenosis. *Journal*
589 *of Tissue Engineering, 7*, 2041731416683745.
590 Liu, H., Li, W., Wen, W., Luo, B., Liu, M., Ding, S., & Zhou, C. (2017). Mechanical properties and
591 osteogenic activity of poly(l-lactide) fibrous membrane synergistically enhanced by chitosan
592 nanofibers and polydopamine layer. *Mater Sci Eng C Mater Biol Appl, 81*, 280-290.
593 Liu, Y., Cui, H., Zhuang, X., Wei, Y., & Chen, X. (2014). Electrospinning of aniline pentamer-graft-
594 gelatin/PLLA nanofibers for bone tissue engineering. *Acta Biomaterialia, 10*(12), 5074-5080.
595 LogithKumar, R., KeshavNarayan, A., Dhivya, S., Chawla, A., Saravanan, S., & Selvamurugan, N. (2016).
596 A review of chitosan and its derivatives in bone tissue engineering. *Carbohydrate Polymers, 151*,
597 172-188.
598 Lynge, M. E., van der Westen, R., Postma, A., & Städler, B. (2011). Polydopamine—a nature-inspired
599 polymer coating for biomedical science. *Nanoscale, 3*(12), 4916-4928.
600 Ma, X., Wu, G., Dai, F., Li, D., Li, H., Zhang, L., & Deng, H. (2021). Chitosan/polydopamine layer by
601 layer self-assembled silk fibroin nanofibers for biomedical applications. *Carbohydrate Polymers,*
602 *251*, 117058.
603 Nie, G., Li, Z., Lu, X., Lei, J., Zhang, C., & Wang, C. (2013). Fabrication of polyacrylonitrile/CuS
604 composite nanofibers and their recycled application in catalysis for dye degradation. *Applied*
605 *Surface Science, 284*, 595-600.
606 Nieto, C., Vega, M. A., Enrique, J., Marcelo, G., & Martín Del Valle, E. M. (2019). Size Matters in the
607 Cytotoxicity of Polydopamine Nanoparticles in Different Types of Tumors. *Cancers, 11*(11), 1679.
608 Norowski Jr, P. A., Fujiwara, T., Clem, W. C., Adatrow, P. C., Eckstein, E. C., Haggard, W. O., &
609 Bumgardner, J. D. (2015). Novel naturally crosslinked electrospun nanofibrous chitosan mats for
610 guided bone regeneration membranes: material characterization and cytocompatibility. *Journal*
611 *of Tissue Engineering and Regenerative Medicine, 9*(5), 577-583.
612 Ouerghemmi, S., Degoutin, S., Tabary, N., Cazaux, F., Maton, M., Gaucher, V., Janus, L., Neut, C., Chai,
613 F., Blanchemain, N., & Martel, B. (2016). Triclosan loaded electrospun nanofibers based on a
614 cyclodextrin polymer and chitosan polyelectrolyte complex. *International Journal of*
615 *Pharmaceutics, 513*(1), 483-495.

Pan, P., Chen, X., Metavarayuth, K., Su, J., & Wang, Q. (2018). Self-assembled supramolecular systems for bone engineering applications. *Current Opinion in Colloid & Interface Science, 35*, 104-111.

Pattnaik, S., Nethala, S., Tripathi, A., Saravanan, S., Moorthi, A., & Selvamurugan, N. (2011). Chitosan scaffolds containing silicon dioxide and zirconia nano particles for bone tissue engineering. *International Journal of Biological Macromolecules, 49*(5), 1167-1172.

Ranganathan, S., Balagangadharan, K., & Selvamurugan, N. (2019). Chitosan and gelatin-based electrospun fibers for bone tissue engineering. *International Journal of Biological Macromolecules, 133*, 354-364.

Ryu, J., Ku, S. H., Lee, H., & Park, C. B. (2010). Mussel-Inspired Polydopamine Coating as a Universal Route to Hydroxyapatite Crystallization. *Advanced Functional Materials, 20*(13), 2132-2139.

Sainitya, R., Sriram, M., Kalyanaraman, V., Dhivya, S., Saravanan, S., Vairamani, M., Sastry, T. P., & Selvamurugan, N. (2015). Scaffolds containing chitosan/carboxymethyl cellulose/mesoporous wollastonite for bone tissue engineering. *International Journal of Biological Macromolecules, 80*, 481-488.

Salerno, A., Fernández-Gutiérrez, M., San Román del Barrio, J., & Domingo, C. (2015). Bio-safe fabrication of PLA scaffolds for bone tissue engineering by combining phase separation, porogen leaching and scCO2 drying. *The Journal of Supercritical Fluids, 97*, 238-246.

Saravanan, S., Nethala, S., Pattnaik, S., Tripathi, A., Moorthi, A., & Selvamurugan, N. (2011). Preparation, characterization and antimicrobial activity of a bio-composite scaffold containing chitosan/nano-hydroxyapatite/nano-silver for bone tissue engineering. *International Journal of Biological Macromolecules, 49*(2), 188-193.

Shahbazarab, Z., Teimouri, A., Chermahini, A. N., & Azadi, M. (2018). Fabrication and characterization of nanobiocomposite scaffold of zein/chitosan/nanohydroxyapatite prepared by freeze-drying method for bone tissue engineering. *International Journal of Biological Macromolecules, 108*, 1017-1027.

Shalumon, K. T., Sowmya, S., Sathish, D., Chennazhi, K. P., Nair, S. V., & Jayakumar, R. (2013). Effect of incorporation of nanoscale bioactive glass and hydroxyapatite in PCL/chitosan nanofibers for bone and periodontal tissue engineering. *J Biomed Nanotechnol, 9*(3), 430-440.

Sharifi, F., Atyabi, S. M., Norouzian, D., Zandi, M., Irani, S., & Bakhshi, H. (2018). Polycaprolactone/carboxymethyl chitosan nanofibrous scaffolds for bone tissue engineering application. *International Journal of Biological Macromolecules, 115*, 243-248.

Shin, Y. M., Jun, I., Lim, Y.-M., Rhim, T., & Shin, H. (2013). Bio-inspired Immobilization of Cell-Adhesive Ligands on Electrospun Nanofibrous Patches for Cell Delivery. *Macromolecular Materials and Engineering, 298*(5), 555-564.

Sobocinski, J., Laure, W., Taha, M., Courcot, E., Chai, F., Simon, N., Addad, A., Martel, B., Haulon, S., Woisel, P., Blanchemain, N., & Lyskawa, J. (2014). Mussel Inspired Coating of a Biocompatible Cyclodextrin Based Polymer onto CoCr Vascular Stents. *ACS Applied Materials & Interfaces, 6*(5), 3575-3586.

Tsai, W.-B., Chen, W.-T., Chien, H.-W., Kuo, W.-H., & Wang, M.-J. (2013). Poly(dopamine) coating to biodegradable polymers for bone tissue engineering. *Journal of Biomaterials Applications, 28*(6), 837-848.

Van Hong Thien, D., Hsiao, S. W., Ho, M. H., Li, C. H., & Shih, J. L. (2013). Electrospun chitosan/hydroxyapatite nanofibers for bone tissue engineering. *Journal of Materials Science, 48*(4), 1640-1645.

Wen, P., Zong, M.-H., Linhardt, R. J., Feng, K., & Wu, H. (2017). Electrospinning: A novel nano-encapsulation approach for bioactive compounds. *Trends in Food Science & Technology, 70*, 56-68.

Yang, X., Chen, X., & Wang, H. (2009). Acceleration of Osteogenic Differentiation of Preosteoblastic Cells by Chitosan Containing Nanofibrous Scaffolds. *Biomacromolecules, 10*(10), 2772-2778.

Zangmeister, R. A., Morris, T. A., & Tarlov, M. J. (2013). Characterization of Polydopamine Thin Films Deposited at Short Times by Autoxidation of Dopamine. *Langmuir, 29*(27), 8619-8628.

667 Zia, Q., Tabassum, M., Meng, J., Xin, Z., Gong, H., & Li, J. (2021). Polydopamine-assisted grafting of
668 chitosan on porous poly (L-lactic acid) electrospun membranes for adsorption of heavy metal
669 ions. *International Journal of Biological Macromolecules, 167*, 1479-1490.

670

671

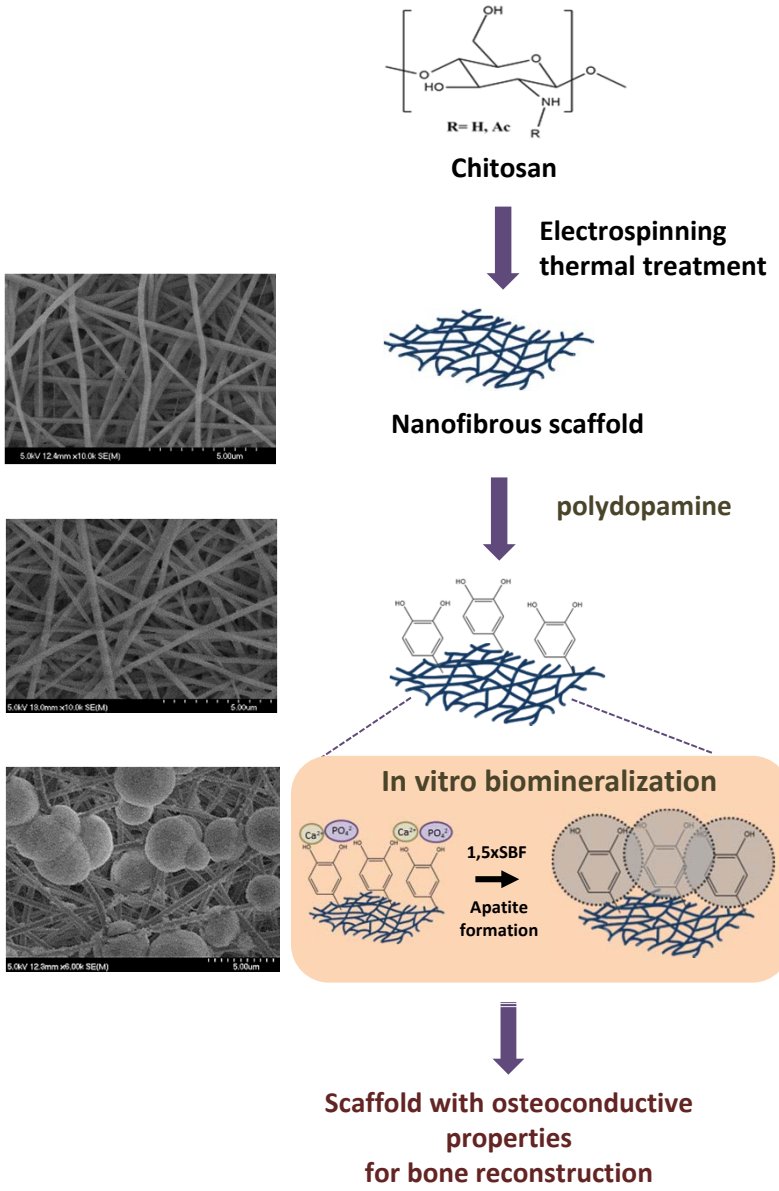
OH
HO
O
NH
R= H, Ac
R
Chitosan
Electrospinning
thermal treatment
Nanofibrous scaffold
polydopamine
In vitro biomineralization
1,5xSBF
Apatite
formation
Scaffold with osteoconductive
properties
for bone reconstruction